

From emission to absorption: the FAST observation of the OH 18-cm lines from the Comet C/2025 A6

Dongyue Jiang¹, Lei Qian^{2,3,4,5}, Minglei Guo², Qiaoli Hao², Menglin Huang², Peng Jiang^{2,3}, Hongfei Liu², Chun Sun², Xingyi Wang², Qingliang Yang², Naiping Yu², Lei Zhao², Yutao Zhao², Liyun Zhang^{1,3,6}, Yichi Zhang⁴, Tongjie Zhang^{7,8} and Zhichen Pan^{2,3,4,5}

¹ Guizhou University, Guiyang 550025, People's Republic of China

² National Astronomical Observatories, Chinese Academy of Sciences, Beijing 100012, People's Republic of China; lqian@nao.cas.cn; panzc@nao.cas.cn

³ Guizhou Radio Astronomical Observatory, Guizhou University, Guiyang 550025, People's Republic of China

⁴ College of Astronomy and Space Sciences, University of Chinese Academy of Sciences, Beijing, 100101, People's Republic of China

⁵ Key Laboratory of Radio Astronomy, Chinese Academy of Sciences, Beijing 100101, People's Republic of China

⁶ International Centre of Supernovae, Yunnan Key Laboratory, Kunming 650216, China

⁷ Institute for Frontiers in Astronomy and Astrophysics, Beijing Normal University, Beijing 102206, People's Republic of China

⁸ School of Physics and Astronomy, Beijing Normal University, Beijing 100875, People's Republic of China Received

20xx month day; accepted 20xx month day

Abstract We observed comet C/2025 A6 with FAST telescope equipped with the ultra-wideband receiver from 23rd October to 8th November 2025 and detected the OH 18-cm lines for the first time. The OH lines underwent a reversal from emission to absorption from 23rd October to 5th November, which is mainly caused by variations in the heliocentric velocity. Through trapezoidal fitting of the OH line profiles, we derive expansion velocities of the water that rise as the heliocentric distance decreases. Based on these results, we estimated the OH production rates of C/2025 A6 for 23rd October, 26th October, 4th November, and 5th November and it presents a significant upward trend.

Key words: methods: observational— comets: general— comets: individual: C/2025 A6

1 INTRODUCTION

The comets spend most of their lives in the outer, frozen regions of the solar system. Their chemical compositions preserve crucial information about the primordial environment and the processes that may dominated the Solar System's formation (A'Hearn 2017; Newburn et al. 1991). When comets approach the Sun, the solar radiation heats their nuclei, causing subsurface ices to sublimate, and releasing gases and various molecules into the space. As the primary volatile in comets, the production rate and abundance of water provide directly insights into the activity of the nucleus and its physical properties (Bockelée-Morvan et al. 2004). Under the solar radiation, the water molecules undergo photodissociation: $h\nu + \text{H}_2\text{O} \Rightarrow \text{OH} + \text{H}$, producing hydroxyl radicals (OH, Crovisier 1989).

Hydroxyl radicals in cometary coma are primarily observed at ultraviolet and radio wavelengths. At radio frequencies, the OH 18-cm lines arise from Λ -doubling and hyperfine transitions within the ground state of the OH radical, distributed near 1612, 1665, 1667, and 1720 MHz (see Table 1). Compared with UV measurements, OH 18-cm lines can be observed from the ground, and less affected by dust extinction. Their narrow profiles provide direct constraints on the gas expansion velocity and kinematic structure of the coma (Bockelée-Morvan et al. 1990). The OH 18-cm line profiles can be used to measure the expansion velocity of water in the cometary coma (Bockelée-Morvan et al. 1990), providing a basis for further studies of the coma's gas dynamics. Since the first detection the OH 18-cm lines from Comet Kohoutek in 1973 (Biraud et al. 1974), long-term ground-based observations have established extensive datasets of water and OH emis-

sions for a wide variety of comets (e.g., Despois et al. 1981; Crovisier et al. 2002; Wang et al. 2017). These studies have extended observations to comets with different orbital periods and have used variations in molecular production rates to investigate cometary outgassing activity. On the other hand, either the emission or the absorption of the OH 18-cm lines from a comet could be observed, where OH is produced by the reaction between the photon and water molecular, requiring the the ultraviolet light with the wavelength shorter than 186 nm (Crovisier 1989).

The Comet C/2025 A6 (Lemmon) is a non-periodic comet. It was discovered by the Mount Lemmon Survey on 3rd January, 2025, and passed closest to Earth on 21st October, 2025, with a geocentric distance of 0.59 AU. It subsequently reached perihelion on 8th November, 2025, at a heliocentric distance of 0.53 AU. Between 3rd January, 2025 and 11th November, 2025, it is in the sky coverage of the Five-hundred-meter Aperture Spherical radio telescope (FAST), which is the largest single-dish radio telescope nowadays in the world. The FAST has been used for comet related studies before (e.g., Chen et al. 2024) with the L-band to search for the molecular spectral lines.

In this work, we present observations of the comet C/2025 A6 with FAST. Section 2 describes the observations. The data processing is mentioned in the Section 3. In Section 4, we discuss the changes of OH line profiles and production rate. The conclusion is presented in Section 5.

Table 1 OH 18-cm hyperfine transitions.

| Transitions | Common designation | Frequency (MHz) |
|---------------------------|--------------------|-----------------|
| $^2\Pi_{3/2} (F = 1 - 2)$ | OH 1612 MHz | 1612.2309 |
| $^2\Pi_{3/2} (F = 1 - 1)$ | OH 1665 MHz | 1665.4018 |
| $^2\Pi_{3/2} (F = 2 - 2)$ | OH 1667 MHz | 1667.3590 |
| $^2\Pi_{3/2} (F = 2 - 1)$ | OH 1720 MHz | 1720.5299 |

2 OBSERVATIONS

The observations of C/2025 A6 were performed with FAST (Nan et al. 2011) on 23rd and 26th October and from 3rd to 8th November in this year. The details can be found in Table 2. It is worth noting that the C/2025 A6 moved very quickly, all observations were conducted in the user-defined mode.

In order to observe the OH 18-cm lines at ~ 1700 MHz, the ultra-wideband (UWB) receiver (Zhang et al. 2023) covering 0.5–3.3 GHz was used. This testing receiver is not cooled and with a system temperature between 89 to 130 K. At the spectra frequency (~ 1660 MHz), the beam size is around $2.5'$. A photo of the comet with the size of FAST beam showing that the



Fig. 1 Optical image of comet C/2025 A6 obtained on 21st October 2025 (18:35–18:50, UTC+8) with the 70-cm UCASST telescope. The image combines 5-min exposures in each of the *R*, *V*, and *B* filters and shows a coma with an apparent diameter of ~ 8 – 10 arcmin. The telescope is equipped with a 2048×2048 detector with a pixel size of $13.5 \mu\text{m}$, providing a field of view of about $20.8' \times 20.8'$, at the time of the observation, $1'$ corresponds to a projected scale of $\sim 25,700$ km at the comet.

nuclei can be fully covered (Figure 1). Previous tests have shown excellent agreement between the OH flux densities and velocities measured with the FAST UWB receiver and those obtained with the Arecibo 300 m telescope (Zhang et al. 2023).

The data from the UWB receiver were separated into four sub-bands, being 0–1100, 800–1900, 1600–2700 and 2400–3500 MHz, respectively. There are 1,048,576 channels in every sub-band, corresponding to a channel width of 1049 Hz. For OH 18-cm lines, the velocity resolution is approximately 0.19 km s^{-1} . The four polarizations were recorded with an integration time of 1 s. The noise calibration signal was injected with noise diodes for 1 second and stopped for 9 seconds in every 10 seconds during the observation. The noise temperatures of the calibration signal injected to the two polarization channels are 16 and 18 K, respectively.

For fast-moving targets such as the comet, we tracked the comet along its predicted trajectory by updating the telescope pointing every 0.1 s during the observation. In order to find any possible background sources which may affect the comet's spectra, positions around the comet were also observed in the observation on November 6th. These positions were at least $3'$ off the comet nuclei.

3 DATA REDUCTION

Due to the limitation of sideband suppression of the UWB, only the bands 500–950, 950–1750, 1750–2550,

Table 2 Ephemeris Parameters and Observations of Comet C/2025 A6.

| Start Time (UTC) | R.A. (h:m:s) | Dec. (d:m:s) | $\langle r \rangle$ (AU) | $\langle \dot{r} \rangle$ (km s $^{-1}$) | $\langle \Delta \rangle$ (AU) | $\langle \dot{\Delta} \rangle$ (km s $^{-1}$) | G (KJy $^{-1}$) | Total times (s) | Trajectory |
|---------------------|-----------------|-----------------|-----------------------------|--|----------------------------------|---|-----------------------|--------------------|-------------|
| 2025/10/23 06:30:00 | 14:53:49.44 | +24:36:16.3 | 0.65 | -22.39 | 0.60 | 13.41 | 12.5 | 3000 | Tracking-On |
| 2025/10/26 03:35:00 | 15:31:52.58 | +16:47:47.8 | 0.61 | -19.85 | 0.64 | 29.05 | 12.6 | 10200 | On-Off |
| 2025/11/03 04:44:00 | 16:36:05.31 | -01:25:22.0 | 0.54 | -9.34 | 0.85 | 55.01 | 10.0 | 2400 | Tracking-On |
| 2025/11/04 04:52:00 | 16:40:51.08 | -03:10:07.7 | 0.54 | -7.65 | 0.88 | 56.54 | 10.5 | 4200 | On-Off |
| 2025/11/05 05:01:00 | 16:45:05.35 | -04:48:38.0 | 0.54 | -5.94 | 0.91 | 57.67 | 10.0 | 2760 | On-Off |
| 2025/11/06 05:09:00 | 16:48:50.68 | -06:21:10.8 | 0.53 | -3.01 | 0.97 | 58.89 | 9.5 | 1560 | Multi-point |
| 2025/11/07 05:17:00 | 16:52:09.97 | -07:48:16.1 | 0.53 | -2.37 | 0.98 | 59.10 | 10.0 | 2880 | Tracking-On |
| 2025/11/08 05:27:00 | 16:55:05.90 | -09:10:25.3 | 0.53 | -0.55 | 1.01 | 59.40 | 9.5 | 2220 | Tracking-On |

Notes. The second and third columns list the astrometric right ascension and declination at the beginning of each observation, in the J2000 reference frame. $\langle r \rangle$ represents the average heliocentric distance during observation, $\langle \dot{r} \rangle$ is the average rate of change of the heliocentric distance. $\langle \Delta \rangle$ is the average distance between the comet and the observatory during the observation, and $\langle \dot{\Delta} \rangle$ represents the average rate of change of the comet–observatory distance during the observation. G is the gain corresponding to the observation.

and 2550–3300 MHz were used (Zhang et al. 2023). The OH 18-cm lines are around 1612 to 1720 MHz. Thus, only the spectra in such frequency range were used in our study. For each cycle, the temperature corresponding to the measured power is determined by differencing the spectral line data acquired with open and closed noise diode, followed by calibrating the resulting power values of all spectral lines into temperature. The calibrated spectral data are processed using the astronomical data processing software GILDAS/CLASS¹. For all observations, a second-order polynomial baseline was fitted and subtracted over a velocity span of 60 km s $^{-1}$ around the line, excluding the channels containing line emission, absorption features, or identifiable RFI.

The spectra were then smoothed with a two-channel boxcar window, yielding a velocity resolution of about 0.38 km s $^{-1}$. All spectra were combined with a sigma-weighted averaging.

We performed Gaussian fitting on all spectra with clear detections to obtain the integrated intensity, line-center velocity, FWHM, and peak amplitude of the OH 18-cm lines. We also applied a trapezoidal fitting procedure to the 1667 MHz spectra of the four observations with detections (23rd October, 26th October, 4th November and 5th November) in order to derive the half-width of the trapezoidal base. The derived parameters are summarized in Table 3.

For whom may interested in the conversion from the brightness temperature to the flux with FAST data, the details can be found in appendix A.

4 RESULTS AND DISCUSSION

During four observing epochs on 23rd October, 26th October, 4th November, and 5th November, either emission or absorption of the 1667 MHz line was detected.

4.1 Change of OH 18-cm Lines from Emission to Absorption

In our observations, the OH 18-cm lines exhibit a clear evolution from emission to absorption. During the first two observing epochs, the OH lines are detected in emission in both the 1665 and 1667 MHz transitions, with corresponding velocities of 13.4 km s $^{-1}$ and 28.9 km s $^{-1}$, respectively. In subsequent observations, the lines appear in absorption in both main lines, with a stronger signal at 1667 MHz. The corresponding line-of-sight velocities are 54.0 km s $^{-1}$, 56.3 km s $^{-1}$, and 57.0 km s $^{-1}$ on 3rd November, 4th November and 5th November, respectively. The fitted line-center velocities are consistent with the expected radial velocity of the comet relative to the telescope at each observing epoch, confirming the cometary origin of the detected signals. No distinct OH signal is detected during the observations from 6th to 8th November within the expected velocity range.

The observed transition of the OH 18-cm lines from emission to absorption indicates a change in the excitation conditions of the OH ground-state Λ -doublet population. In the cometary coma, these level populations are controlled primarily by resonant solar ultraviolet fluorescence, and the resulting inversion parameter depends on the comet’s heliocentric radial velocity.

The OH $A^2\Sigma^+ - X^2\Pi$ (0 – 0) band near 3086 Å is pumped by a dense set of intrinsically narrow ro-vibrational transitions. The corresponding Doppler shift can be approximated as

$$\Delta\lambda \simeq \lambda \frac{v_h}{c}, \quad (1)$$

such that at $\lambda = 3086$ Å, a heliocentric radial velocity of $v_h = 10$ km s $^{-1}$ corresponds to a wavelength of $\Delta\lambda \simeq 0.1$ Å. At these wavelengths, the solar Fraunhofer spectrum is strongly structured on scales of order 0.1 Å, comparable

¹ <https://www.iram.fr/IRAMFR/GILDAS/>

Table 3 The 18cm OH spectral characteristics of C/2025 A6.

| Date (UT) | Lines | RMS (K) | Area (K km s ⁻¹) | <i>i</i> | T_{bg} (K) | S ($\times 10^{-1}$ Jy km s ⁻¹) | v (km s ⁻¹) | FWHM (km s ⁻¹) | T_{peak} (K) | $v_p + v_d$ (km s ⁻¹) |
|------------|-------|---------|------------------------------|----------|---------------------|--|---------------------------|----------------------------|-----------------------|-----------------------------------|
| 2025/10/23 | 1665 | 0.07 | 2.1±0.1 | 0.45 | 3.3 | 1.7±0.1 | 13.4±0.1 | 3.4±0.2 | 0.59 | 2.4±0.3 |
| | 1667 | 0.07 | 3.9±0.1 | | | 3.1±0.1 | 13.3±0.1 | 3.1±0.1 | 1.21 | 2.4±0.1 |
| 2025/10/26 | 1665 | 0.06 | 2.3±0.1 | 0.51 | 3.5 | 1.8±0.1 | 28.8±0.1 | 3.5±0.2 | 0.61 | 2.9±0.6 |
| | 1667 | 0.06 | 4.8±0.1 | | | 3.8±0.1 | 29.0±0.1 | 3.4±0.1 | 1.33 | 2.6±0.1 |
| 2025/11/03 | 1665 | 0.08 | -0.2±0.1 | -0.27 | 3.1 | -0.2±0.1 | 54.0±0.1 | 0.7±0.3 | -0.23 | - |
| | 1667 | 0.09 | -0.4±0.1 | | | -0.4±0.1 | 53.5±0.1 | 1.1±0.2 | -0.34 | - |
| 2025/11/04 | 1665 | 0.12 | -0.5±0.1 | -0.37 | 3.1 | -0.5±0.1 | 55.9±0.2 | 1.3±0.3 | -0.38 | - |
| | 1667 | 0.09 | -1.4±0.2 | | | -1.3±0.2 | 56.4±0.2 | 3.2±0.4 | -0.40 | 3.6±0.8 |
| 2025/11/05 | 1665 | 0.20 | -0.6±0.2 | -0.33 | 3.1 | -0.7±0.2 | 57.8±0.6 | 3.9±1.1 | -0.16 | - |
| | 1667 | 0.09 | -1.3±0.2 | | | -1.4±0.2 | 57.0±0.3 | 3.9±0.6 | -0.33 | 3.9±0.9 |

Notes. Column 2 represents the spectral lines observed in the corresponding frequency range; Column 3 is the 1σ noise of the observed spectra with the channel width 0.38 km s^{-1} ; Column 4, 8, 9, 10 are derived from Gaussian fitting, representing the integrated intensity, the position of the center of the line obtained through fitting, the full width at half height, and the peak temperature obtained through fitting, respectively; Column 5 is the inversion of ground state of (Schleicher & A'Hearn 1988); Column 7 represents the corresponding flux; Column 11 is the half-length of the base, derived from trapezoidal fitting which represents the sum of the velocities of the parent and daughter molecules.

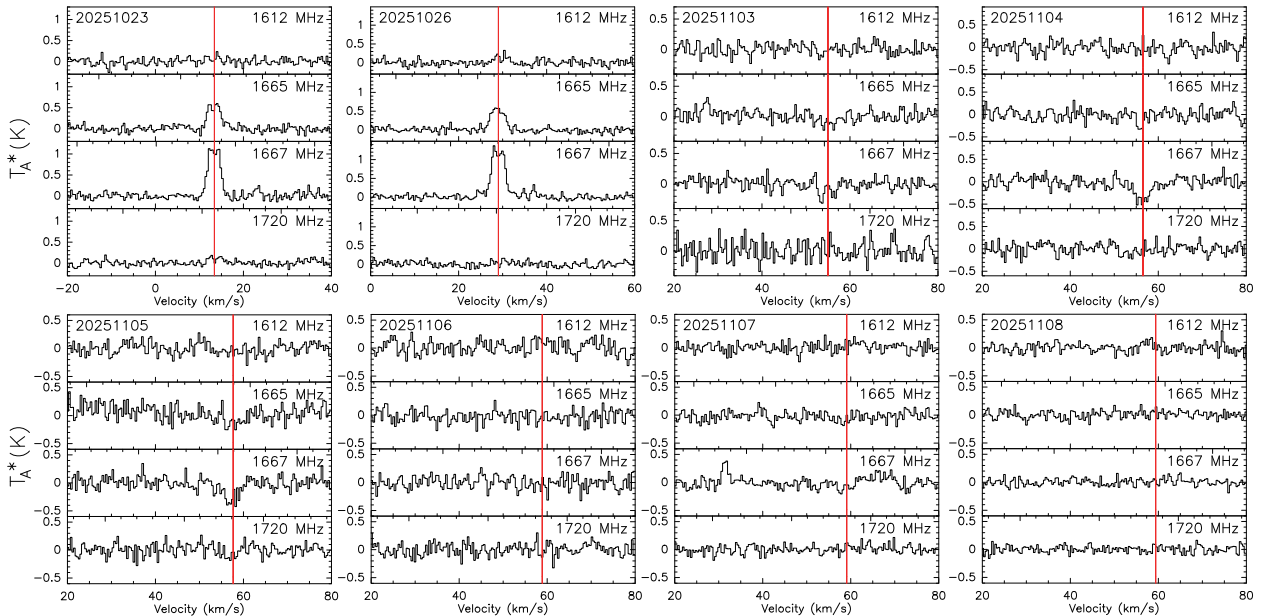


Fig. 2 The OH 18-cm lines obtained on the individual observing dates. All spectra were processed with a two-channel boxcar smoothing, yielding a final velocity resolution of 0.38 km s^{-1} . The OH main lines show emission on 23rd and 26th October, and transition to absorption starting on 3 November. No significant OH signal was detected during 6–8th November. The red vertical line indicates the comet's line-of-sight radial velocity relative to the observatory, as computed from the JPL Horizons system.

to the Doppler shifts induced by heliocentric radial velocities of a few km s^{-1} (see Fig. 2 of Schleicher & A'Hearn 1982).

Consequently, modest heliocentric radial velocity variations during the observing period can alter the OH pumping rate and drive the inversion parameter of the ground-state Λ -doublet across zero. Against the Galactic back-

ground continuum, this leads to a transition in the observed OH 18-cm line profiles from emission to absorption (Despois et al. 1981). Using the inversion curves of Schleicher & A'Hearn (1988), we derived the inversion parameter i at the heliocentric radial velocity of each epoch and compared it with the observed line profiles. The emission detected at early epochs and the absorption observed

at later times are consistent with positive ($i > 0$) and negative ($i < 0$) inversion, respectively. The absence of a clear OH detection in the final observing epochs likely indicates that the inversion parameter was close to zero.

4.2 Water Expansion Velocities from OH Lines

The OH coma is commonly described using a spherically symmetric, steady-state, and isotropic outflow model, in which OH is treated as a secondary product of H₂O photodissociation. The velocity of OH molecules is determined by the expansion velocity of the parent gas, v_p , combined with an additional ejection velocity due to photodissociation, v_d (Bockelee-Morvan & Gerard 1984; Crovisier et al. 2002). The OH 18-cm lines profiles can be well reproduced by trapezoidal fitting, where the width of the lower base corresponds to $2(v_d + v_p)$. This trapezoidal profile model has been widely applied in cometary OH line studies (Drozdovskaya et al. 2023; Li et al. 2025; Sakai et al. 2025). Although OH line profiles always display asymmetries due to anisotropic outgassing toward the Sun or Earth (Li et al. 2025), such effects have only a limited impact on the determination of the lower-base width (Bockelee-Morvan & Gerard 1984). In this work, we adopt a value of $v_d = 0.95 \text{ km s}^{-1}$ to represent the ejection velocity of OH radicals following the photodissociation of H₂O, based on the analyses presented in (Crovisier et al. 2002; Tseng et al. 2007). This value is consistent with the typical OH ejection speeds reported in previous cometary studies (Crovisier 1989; Bockelée-Morvan et al. 1990). The resulting values of $v_d + v_p$ derived from the symmetric trapezoidal fits are listed in Table 3.

4.3 The estimate of OH production rate

The OH production rate can be estimated by (Schloerb & Gerard 1985; Bockelée-Morvan et al. 1990):

$$f\Gamma = 2.33 \times 10^{34} \frac{\Delta^2 S}{iT_{\text{bg}}} \quad (2)$$

and

$$Q_{\text{OH}} = \frac{\Gamma}{\tau_{\text{OH}}}, \quad (3)$$

where Γ is total number of OH radicals in the coma, S is the integrated intensity of the 1667 MHz line in units of Jy km s⁻¹, i is the inversion of the ground state, and Δ is the geocentric distance of the comet in AU. T_{bg} denotes the background temperature in the unit of K, τ_{OH} is the OH lifetime, and f is correction factor. For τ_{OH} , it can be expressed as: $\tau_{\text{OH}} = \tau_{\text{OH}(1\text{AU})} \times r_h^2$ (Wang et al. 2017; Sakai et al. 2025), and $\tau_{\text{OH}(1\text{AU})}$ was estimated as $1.1 \times 10^5 \text{ s}$ from Bockelée-Morvan et al. (1990), where the r_h is the heliocentric distance of the

comet. Following the method of Crovisier et al. (2002), we estimated T_{bg} using the 1420 MHz brightness temperature distribution. The 1420 MHz map was obtained from the NASA/LAMBDA² Stockert–Villa-Elisa all-sky survey (Reich 1982; Reich & Reich 1986; Testori et al. 2001), and the corresponding background temperature T_{bg} is listed in Table 3. The inversion of ground state at the corresponding coma velocity is obtained from (Schleicher & A’Hearn 1988) and listed in Table 3.

Since the FAST beam is considerably smaller than the characteristic size of the OH coma, a beam-size correction is required to account for flux losses outside the beam. We therefore apply the correction factor f to convert the observed number of OH radicals within the beam to the total OH population in the coma. It can be expressed as:

$$f = \frac{\int_0^{+\infty} N(\rho) \omega(\rho) \rho d\rho}{\int_0^{+\infty} N(\rho) \rho d\rho} \quad (4)$$

where $N(\rho)$ is the OH column density distribution derived from Haser model. The expansion velocity v_p is derived from the trapezoidal fits, and the photodissociation lifetime of H₂O at 1 AU is adopted as $4.6 \times 10^4 \text{ s}$ (Huebner et al. 1992), also scaling as r_h^2 . The beam weighting function $\omega(\rho)$ is assumed to be Gaussian, with a FWHM of 2.5 arcmin.

For small heliocentric distances, the inversion of the OH ground state is quenched by the collision of ions and electrons. Neglecting the contribution of the quenched region will lead to an underestimate of the OH production rate. However, owing to the small FAST beam, which is comparable in size to the quenching region, the iterative quenching correction fails to converge for our observational configuration. Details are provided in Appendix B.

When only the beam correction is applied, the derived Q_{OH} values serve as lower limits, with value of $(1.0 \pm 0.1) \times 10^{29}$, $(1.2 \pm 0.1) \times 10^{29}$, $(1.4 \pm 0.3) \times 10^{29}$, and $(1.5 \pm 0.4) \times 10^{29} \text{ s}^{-1}$ for 23rd October, 26th October, 4th November, and 5th November, respectively. The Q_{OH} production rate basically increases as the heliocentric distance decreases. The water production rate of comet can be approximated as $Q_{\text{H}_2\text{O}} = 1.1 Q_{\text{OH}}$ (e.g., Sakai et al. 2025; Li et al. 2025).

5 CONCLUSIONS

We present FAST observations of the OH 18-cm lines in comet C/2025 A6 obtained between 23rd October and 8th November 2025. Our main results and conclusions can be summarized as follows:

1. We confirm that the detected OH 18-cm signals originate from the cometary coma. This conclusion is supported by

² <https://lambda.gsfc.nasa.gov/product>

(i) the agreement between the fitted line-center velocities and radial velocity of the comet relative to the telescope, and (ii) the On–Off observations, in which no emission is detected at the offset positions along the comet’s trajectory. We detected the OH main lines in emission on 23rd and 26th October and in absorption on 3rd to 5th November. The observed emission-to-absorption transition is consistent with the dependence of the OH inversion parameter on heliocentric radial velocity through the Swings effect, which can drive the inversion parameter across zero.

2. We fitted the detected OH line profiles with a trapezoidal model and derived the corresponding parent expansion velocities. The results show that the expansion velocity increases as the heliocentric distance decreases, in agreement with expectations for solar-driven cometary outgassing.

3. Using the measured 1667 MHz line intensities and applying beam-size and quenching corrections, we estimate a plausible range of OH production rates and derive lower limits on Q_{OH} . The results show a general increase with decreasing heliocentric distance.

Future observations sampling multiple positions across the coma, or coordinated observations using beams of different sizes, will mitigate systematic uncertainties associated with collisional quenching and provide more robust constraints on Q_{OH} .

Acknowledgements This work is supported by the National Key R & D Program of China No. 2025SKA0140100, No. 2022YFC2205202, No. 2020SKA0120100, and the National Natural Science Foundation of China (NSFC, Grant Nos. 12373032, 12003047, 11773041, U2031119, 12173052, and 12173053). Both Lei Qian and Zhichen Pan were supported by the Youth Innovation Promotion Association of CAS (id. 2018075, Y2022027, and 2023064) and the CAS “Light of West China” Program. Hongfei Liu has been supported by the National Natural Science Foundation of China (NSFC) under No.12273072. Liyun Zhang has been supported by the Science and Technology Program of Guizhou Province under project No.QKHPTRC-ZDSYS[2023]003 and QKHFQ[2023]003. FAST is a Chinese national mega-science facility, operated by National Astronomical Observatories, Chinese Academy of Sciences. This work made use of the data from FAST (Five-hundred-meter Aperture Spherical radio Telescope). We thank Prof. Oleg Smirnov and his group at MeerKAT for very helpful discussions. We also acknowledge the support of the University of Chinese Academy of Sciences and the use of its 70 cm telescope.

Royal Society of London Series A, 375, 20160261 1
 Biraud, F., Bourgois, G., Crovisier, J., et al. 1974, A&A, 34, 163 1
 Bockelée-Morvan, D., Crovisier, J., & Gérard, E. 1990, A&A, 238, 382 1, 5
 Bockelée-Morvan, D., Crovisier, J., Mumma, M. J., & Weaver, H. A. 2004, in Comets II, ed. M. C. Festou, H. U. Keller, & H. A. Weaver, 391 1
 Bockelée-Morvan, D., & Gerard, E. 1984, A&A, 131, 111 5
 Chen, L.-F., Tsai, C.-W., Li, J.-Y., et al. 2024, Research in Astronomy and Astrophysics, 24, 105008 2
 Crovisier, J. 1989, A&A, 213, 459 1, 2, 5
 Crovisier, J., Colom, P., Gérard, E., Bockelée-Morvan, D., & Bourgois, G. 2002, A&A, 393, 1053 2, 5
 Despois, D., Gerard, E., Crovisier, J., & Kazes, I. 1981, A&A, 99, 320 2, 4, 7
 Drozdovskaya, M. N., Bockelée-Morvan, D., Crovisier, J., et al. 2023, A&A, 677, A157 5
 Huebner, W. F., Keady, J. J., & Lyon, S. P. 1992, Ap&SS, 195, 1 5
 Jiang, P., Yue, Y., Gan, H., et al. 2019, Science China Physics, Mechanics, and Astronomy, 62, 959502 7
 Li, J., Shi, X., Shi, J., et al. 2025, A&A, 701, A204 5, 7
 Nan, R., Li, D., Jin, C., et al. 2011, International Journal of Modern Physics D, 20, 989 2
 Newburn, Jr., R. L., Neugebauer, M., & Rahe, J., eds. 1991, Astrophysics and Space Science Library, Vol. 167, Comets in the Post-Halley ERA - Volume 1; Volume 2 1
 Reich, P., & Reich, W. 1986, A&AS, 63, 205 5
 Reich, W. 1982, A&AS, 48, 219 5
 Sakai, N., Poshayachinda, S., Sugiyama, K., et al. 2025, Planetary Science Journal, 6, 261 5
 Schleicher, D. G., & A'Hearn, M. F. 1982, ApJ, 258, 864 4
 Schleicher, D. G., & A'Hearn, M. F. 1988, ApJ, 331, 1058 4, 5
 Schloerb, F. P., & Gerard, E. 1985, AJ, 90, 1117 5
 Testori, J. C., Reich, P., Bava, J. A., et al. 2001, A&A, 368, 1123 5
 Tseng, W.-L., Bockelée-Morvan, D., Crovisier, J., Colom, P., & Ip, W.-H. 2007, A&A, 467, 729 5
 Wang, Z., Chen, X., Gao, F., et al. 2017, AJ, 154, 249 2, 5
 Zhang, C.-P., Jiang, P., Zhu, M., et al. 2023, Research in Astronomy and Astrophysics, 23, 075016 2, 3, 7

References

A'Hearn, M. F. 2017, Philosophical Transactions of the

Appendix A: FROM ANTENNA TEMPERATURE TO FLUX FOR FAST UWB DATA

The antenna brightness temperature was converted to flux density by using:

$$S = \frac{T_A^*}{G} \quad (\text{A.1})$$

Where the G is the antenna gain in the unit of K Jy^{-1} , and T_A^* is the antenna brightness temperature in the unit of K . The antenna gain can be derived by:

$$G = \eta G_0 \quad (\text{A.2})$$

Here, η represents the telescope's efficiency, and G_0 is the theoretical gain based on the geometrical illumination area. We adopt the value of the Gain at the 1650 MHz from (Zhang et al. 2023), according to the zenith angle (ZA) which they detected derive the corresponding $G_0 \approx 19.6 \text{ K Jy}^{-1}$, then get the actual gain through the relationship between ZA and η (Jiang et al. 2019). The result was shown in Table 2.

Appendix B: THE OH PRODUCTION RATE WITH QUENCHING

When considering the quenching effect, we assume that the inversion factor becomes $i = 0$ for $r < r_q$, so that OH radicals within this region do not contribute to the observable 18-cm signal (Despois et al. 1981), and the factor f can be written as:

$$f = \frac{\int_0^{+\infty} N'(\rho) \omega(\rho) \rho d\rho}{\int_0^{+\infty} N(\rho) \rho d\rho} \quad (\text{B.1})$$

Where the $N'(\rho)$ is the column density distribution after subtracted the sphere with radius r_q . The quenching radius r_q can be expressed as $r_q = r_q^* r_h \sqrt{Q_{\text{OH}}/10^{29}}$ (e.g., Li et al. 2025). Adopting $r_q^* = 47,000$ following Li et al. (2025) results in unstable convergence. We therefore adopt a reduced value of r_q^* to ensure convergence. With this treatment, the derived Q_{OH} values for 23rd October, 26th October, 4th November, and 5th November are $(2.4 \pm 0.3) \times 10^{29}$, $(2.8 \pm 0.3) \times 10^{29}$, $(3.6 \pm 0.5) \times 10^{29}$, and $(3.9 \pm 1.0) \times 10^{29} \text{ s}^{-1}$, respectively.